Langmuir
Article
pubs.acs.org/Langmuir

Self-Catalytic Sol−Gel Synergetic Replication of Uniform Silica Nanotubes Using an Amino Acid Amphiphile Dynamically Growing Fibers as Template

Sheng Lei, Jing Zhang, Jiarui Wang, and Jianbin Huang*

Beijing National Laboratory for Molecular Sciences (BNLMS), State Key Laboratory for Structural Chemistry of Unstable and Stable Species, College of Chemistry and Molecular Engineering, Peking University, Beijing 100871, China

Received September 8, 2009. Revised Manuscript Received November 24, 2009

The aggregation behavior of a novel histidine derivative surfactant *N*-dodecanoyl-L-histidine (DHis) in aqueous solution was investigated. By mixing with cationic/anionic surfactant, an interesting phase transition over time from transparent homogeneous solution to jelly and finally to fibrous floccules was observed with aggregates growth taken place in the systems. Making use of the growing fibrous structures in the DHis/DTEAB and DHis/SDS systems as surface charge tunable dynamic template, we achieved sol−gel replication of silica and titania nanotubes in mild conditions, respectively. The possible mechanism underlying the formation of silica nanotubes was proved to be synergistically self-catalyzed hydrolysis and condensation of silica precusors depositing on the template surface. In particular, by optimizing the sol−gel process, silica nanotubes with tunable sizes in diameter and uniform wall thickness could be obtained in high yield. The large specific surface area and peculiar photoluminescence property of the silica nanomaterials indicated that the synthetic nanotubes were well-defined in both morphology and physical properties. Importantly, this fibrous aggregates could be universally used in opposite charged inorganic precursors to accomplish inorganic oxide nanotubes via sol−gel replication process, which may provide a general route for the construction of one-dimensional nanostructures in aqueous media.

Introduction

One-dimensional nanostructures have proven to be of extraordinary value in chemistry,[1] biochemistry,[2] and material science.[3] Nature has developed numerous astonishing approaches to generate 1D nanostructures performing diverse biological functions. How to mimic and understanding the biological self-assembly process of natural materials is of great significance. Consequently, considerable attention has been focused on the preparation of 1D materials to meet certain requirements.[4] Among them, the self-assembly process exhibits fascinating inherent advantages such as low-temperature fabrication and easy modification. Examples on self-assembled structures have been reported such as tubes[5] and fibers[6] based on hydrogen bonding,[7] aromatic stacking interactions,[8] and hydrophobic effect.[9] This strategy involves fabrication of organic molecular aggregates such as macromolecule complex, surfactants hydrogel or organogel, and biomaterials (e.g., cellulose or membrane protein). To name a few, Gazit et al. reported the unique properties of peptide nanotubes and their proteolytic lability and their use as nanometer-scale molds for the casting of silver nanowires.[1e] Shinkai and co-workers utilized organogel to synthesize silica multilayer hollow spheres and chiral tubule structures.[10] Hanabusa et al. made use of organogelators to gel titanium precursor to obtain titania nanotubes.[11] Adachi et al.,[12] Shimizu et al.,[13] and Hartgerink et al.[14] employed their fibers self-assembled from phospholipids and peptide surfactants to prepare silica nanotubes.

Study concerning fibrous aggregates has been noticed and addressed for decades. An early report showed that lithium 12-hydroxystearate could form helical fibrous structures.[15] Thereafter, numerous relevant reports emerged in the systems of deoxycholic acid,[16] amphiphile with rigid segments,[17]

*Corresponding author: e-mail jbhuang@pku.edu.cn; Fax 86-10-62751708; Tel 86-10-62753557.

(1) Guler, M. O.; Stupp, S. I. *J. Am. Chem. Soc.* **2007**, *129*, 12082.
(2) (a) Yan, X.; He, Q.; Wang, K.; Duan, L.; Cui, Y.; Li, J. *Angew. Chem., Int. Ed.* **2007**, *46*, 2431. (b) Khakshoor, O.; Demeler, B.; Nowick, J. S. *J. Am. Chem. Soc.* **2007**, *129*, 5558. (c) Hartgerink, J. D.; Beniash, E.; Stupp, S. I. *Science* **2001**, *294*, 1684. (d) Silva, G. A.; Czeisler, C.; Niece, K. L.; Beniash, E.; Harrington, D. A.; Kessler, J. A.; Stupp, S. I. *Science* **2004**, *303*, 1352. (e) Reches, M.; Gazit, E. *Science* **2003**, *300*, 625.
(3) (a) Datar, A.; Oitker, R.; Zang, L. *Chem. Commun.* **2006**, 1649. (b) Xiao, R.; Cho, S. I.; Liu, R.; Lee, S. B. *J. Am. Chem. Soc.* **2007**, *129*, 4483. (c) Zhou, Y.; Liu, W. J.; Ma, Y.; Wang, H.; Qi, L.; Cao, Y.; Wang, J.; Pei, J. *J. Am. Chem. Soc.* **2007**, *129*, 12386. (d) Yamamoto, Y.; Fukushima, T.; Saeki, A.; Seki, S.; Tagawa, S.; Ishii, N.; Aida, T. *J. Am. Chem. Soc.* **2007**, *129*, 9276.
(4) (a) Greiner, A.; Wendorff, J. H. *Angew. Chem., Int. Ed.* **2007**, *46*, 5670. (b) Hamley, I. W. *Angew. Chem., Int. Ed.* **2007**, *46*, 8128. (c) Demirel, A. L.; Meyer, M.; Schlaad, H. *Angew. Chem., Int. Ed.* **2007**, *46*, 8622. (d) Lee, H. Y.; Nam, S. R.; Hong, J. I. *J. Am. Chem. Soc.* **2007**, *129*, 1040. (e) Xu, Y.; Ye, J.; Liu, H.; Cheng, E.; Yang, Y.; Wang, W.; Zhao, M.; Zhou, D.; Liu, D.; Fang, R. *Chem. Commun.* **2008**, 49.
(5) (a) Wu, D.; Zhi, L.; Bodwell, G. J.; Cui, G.; Tsao, N.; Mullen, K. *Angew. Chem., Int. Ed.* **2007**, *46*, 5417. (b) Hill, J. P.; Jin, W.; Kosaka, A.; Fukushima, T.; Ichihara, H.; Shimomura, T.; Ito, K.; Hashizume, T.; Ishii, N.; Aida, T. *Science* **2004**, *304*, 1481. (c) John, G.; Masuda, M.; Okada, Y.; Yase, K.; Shimizu, T. *Adv. Mater.* **2001**, *13*, 715.
(6) (a) Mankidy, P. J.; Rajagopalan, R.; Foley, H. C. *Chem. Commun.* **2006**, 1139. (b) Kakade, M. V.; Givens, S.; Gardender, K.; Lee, K. H.; Chase, D. B.; Rabolt, J. F. *J. Am. Chem. Soc.* **2007**, *129*, 2777.
(7) (a) Ghadiri, M. R.; Granja, J. R.; Milligan, R. A.; McRee, D. E.; Khazanovich, N. *Nature* **1993**, *366*, 324. (b) Behanna, H. A.; Donners, J. J. J. M.; Gordon, A. C.; Stupp, S. I. *J. Am. Chem. Soc.* **2005**, *127*, 1193. (c) Miravet, J. F.; Escuder, B. *Chem. Commun.* **2005**, 5769.
(8) Che, Y.; Datar, A.; Balakrishnam, K.; Zang, L. *J. Am. Chem. Soc.* **2007**, *129*, 7234.
(9) Won, Y. Y.; Davis, H. T.; Bates, F. S. *Science* **1999**, *283*, 960.
(10) (a) Jung, J. H.; Ono, Y.; Sakurai, K.; Sano, M.; Shinkai, S. *J. Am. Chem. Soc.* **2000**, *122*, 8648. (b) Jung, J. H.; Ono, Y.; Hanbusa, K.; Shinkai, S. *J. Am. Chem. Soc.* **2000**, *122*, 5008.
(11) Kobayashi, S.; Hanabusa, K.; Hamasaki, N.; Kimura, M.; Shirai, H. *Chem. Mater.* **2000**, *12*, 1523.
(12) (a) Adachi, M.; Harada, T.; Harada, M. *Langmiur* **1999**, *15*, 7097. (b) Harada, M.; Adachi, M. *Adv. Mater.* **2000**, *12*, 839.
(13) Ji, Q.; Iwaura, R.; Kogiso, M.; Jung, J. H.; Yoshida, K.; Shimizu, T. *Chem. Mater.* **2004**, *16*, 250.
(14) Yuwono, V. M.; Hartgerink, J. D. *Langmuir* **2007**, *23*, 503.
(15) Tachibana, T.; Kambara, H. *J. Am. Chem. Soc.* **1965**, *87*, 3015.
(16) Ramanathan, N.; Currie, A. L.; Colvin, J. R. *Nature* **1961**, *190*, 779.
(17) Kunitake, T.; Okahata, Y.; Shimomura, M.; Yasunami, S.; Takarabe, K. *J. Am. Chem. Soc.* **1981**, *103*, 5401.

5′-phosphatidylnucleosides,[18] alkylaldonamides,[19] and natural amino acid derivative amphiphiles.[20] They were found to self-assemble into screwed or intertwisted fibrous organized assemblies in solution.

However, the rational synthesis of complex molecules still lacks flexibility and applicability for diverse precursors, primarily because underlying growth mechanisms remain largely hypothetical for biomimetic structures.[21] For instance, there is a current consensus that bio-templated silica materials are produced from the interaction of silica precursors with self-assembling proteins containing amine moieties.[22] Nevertheless, whether the organic matrix is performed or dynamically grown under the influence of the mineralization is still open. To this end, we investigated the bio-inspired silica mineralization process of self-assembled amino acid surfactant *N*-dodecanoyl-L-histidine (DHis) in this work, hoping to shed some light on this question.

Employing histidine derivative surfactant as the key component in this work comes down to the following benefits. First, it derives from natural amino acid, endowing it with environmental benign specificity, i.e., low toxicity and biodegradability. Second, the zwitterionic nature of the headgroup assures the tunable surface charge of the aggregates. Third, the synthesis of DHis is easy and low-cost, adapting to mass production. By simple strategies such as ionic surfactant solubilization, the insoluble DHis molecules could self-assemble into organic fibrous structures in aqueous solution that catalyze the hydrolysis and condensation of silica precursors on the fiber surface. The main advantages of this approach are that it is easily adaptable to large-scale fabrication, and the diameter of the silica nanotubes is tunable through simple variation of incubation temperature. On the basis of experimental results, a coupling mechanism was proposed as the self-catalyzed synergetic growth of silica precursors and dynamic fibrous templates. Furthermore, we successfully prepared titania nanotubes in an opposite charged fiber system made up of DHis and anionic surfactant SDS using a similar strategy, which further confirmed our mechanism and enlarged the application range of this template.

Experimental Section

Materials. Sodium dodecyl sulfate (SDS) and pyrene were purchased from Acros. Cationic quaternary ammonium surfactant dodecyltriethylammonium bromide (DTEAB) was synthesized from 1-bromododecane and triethylamine. The purity of the surfactant was examined by NMR and elementary analysis. L-Histidine was purchased from Alfa Aesar. Tetraethyl silicate (TEOS) was purchased from Sigma-Aldrich, and titanium(IV) *n*-butoxide (TBOT) was received from Alfa Aesar. Other chemicals used in this article were of analytical purity purchased from Beijing Chemical Works. Distilled water was purified through Milli-Q Advantage A10 Ultrapure Water System with an electrical resistance of 18.4 MΩ·cm.

General Instruments. ^{1}H NMR spectra were recorded on a Mecury Plus 300 M (USA) instrument in DMSO-*d* solvent. Analyses of C, H, and N were conducted on an Elementar Vario MICRO CUBE elemental analyzer (Germany).

Synthesis of *N*-Dodecanoyl-L-histidine (DHis). Similar to the previous reports,[23] see corresponding section and Figures S1−S3 in the Supporting Information.

Steady-State Fluorescence Measurement. The fluorescence emission spectra of pyrene dissolved in pH regulated DHis solution were carried out using a FLS 920 spectrofluorometer of Edinburgh Instruments with a monochromated Xe lamp as an exitation source. The temperature of the water-jacketed cell holder was controlled by a thermostat at 45 °C to ensure a homogeneous solution. The emission spectra were recorded from 350 to 450 nm after exitation at 335 nm with the slit widths fixed at 2.5 and 5 nm for the exitation and emission, respectively. The pyrene concentration was fixed at 1×10^{-7} mol/L in all the measurements. Pyrene is a strong hydrophobic probe, and its fluorescence emission spectrum exhibits characteristic five bands in the region of 370−400 nm. The first and third characteristic vibronic peaks of pyrene appeared at ca. 373 and 384 nm, respectively. Specially, the intensity ratio of the first to the third vibronic peaks, i.e., I_1/I_3, is extremely sensitive to the micropolarity surrounding the pyrene molecule and can be taken as a measure for to the polarity of the environment.[24]

Differential Scanning Calorimetry (DSC). The DSC measurements were carried out at 1 °C min^{-1} using a Micro DSC III (Setaram-France) instrument.

Sample Preparation. To obtain a mixed surfactant stabilized fibrous precipitate solution, DTEAB or SDS was added to the DHis aqueous solution to obtain a desired DHis/surfactant molar ratio. Then the solution was heated to 80 °C to become homogeneous and clear. After gradually cooling to room temperature (30 °C), the solution became jellylike, and then with further incubation it finally shrank and precipitated from the solution.

Fabrication of Silica Nanotubes. Typically, DHis (0.0810 g, 0.24 mmol) and DTEAB (0.0210 g, 0.06 mmol) were dissolved in 30 mL of water to obtain a DHis/DTEAB = 8/2, C_t = 10 mmol/L system. Upon heating to 80 °C, a clear homogeneous solution was obtained. After slowly cooling to room temperature (ca. 25 °C), 5% (v/v) TEOS was fed into the stock solution under magnetic stirring. Then the mixed solution was incubated under static conditions in a 30 °C thermostat container. The hydrolysis reaction of TEOS was performed for 24 h. Subsequently, the as-formed silica gel was washed with ethanol for three times and collected after centrifugation. Afterward, the products were dried at 60 °C and moved to a furnace to be calcined. The annealing procedure was performed at a heating rate of 5 °C/min and kept at 550 °C for 3 h to remove surfactants and organic residua. After cooling naturally to room temperature, a large quantity of white powder was obtained as source material.

Production of Titania Nanotubes. Similarly as the process of silica nanotubes fabrication, the procedure involved substituting SDS for DTEAB, adding the same molar of acetyl acetone (ACA) to TBOT as the hydrolysis suppressive agent, washing the raw titania gel with water, and the annealing temperature was set to 500 °C.

Characterization. Field-emission scanning electron microscopy (FESEM) images and energy-dispersive X-ray spectroscopy (EDX) data were taken with a Hitachi S4800 equipped with an EDX facility. Transmission electron microscopy (TEM) images were acquired with JEOL JEM 200 CX under a working voltage of 160 kV. High-resolution TEM (HRTEM) images and selected-area electron diffraction (SAED) patterns were performed with a FEI Tecnai F30 FEG-TEM instrument operated at 300 kV. For the TEM analysis, the samples were deposited on a carbon mesh

(18) Yanagawa, H.; Ogawa, Y.; Furuta, H.; Tsuno, K. *J. Am. Chem. Soc.* **1989**, *111*, 4567.
(19) (a) Fuhrhop, J. H.; Schnieder, P.; Boekema, E.; Helfrich, W. *J. Am. Chem. Soc.* **1988**, *110*, 2861. (b) Fuhrhop, J. H.; Demoulin, C.; Rosenberg, J.; Boettcher, C. *J. Am. Chem. Soc.* **1990**, *112*, 2827.
(20) (a) Imae, T.; Takahashi, Y.; Muramatsu, H. *J. Am. Chem. Soc.* **1992**, *114*, 3414. (b) Luo, X.; Liu, B.; Liang, Y. *Chem. Commun.* **2001**, 1556. (c) Mohanty, A.; Dey, J. *Langmuir* **2004**, *20*, 8452. (d) Das, D.; Dasgupta, A.; Roy, S.; Mitra, R. N.; Debnath, S.; Das, P. K. *Chem.—Eur. J.* **2006**, *12*, 5068. (e) Mohanty, A.; Dey, J. *Langmuir* **2007**, *23*, 1033.
(21) (a) Hukkamaki, J.; Pakkanen, T. T. *Microporous Mesoporous Mater.* **2003**, *65*, 189. (b) Van Bommel, K. J. C.; Shinkai, S. *Langmuir* **2002**, *18*, 4544.
(22) (a) Cha, J. N.; Shimizu, K.; Zhou, Y.; Christiansen, S. C.; Chmelka, B. F.; Stucky, G. D.; Morse, D. E. *Proc. Natl. Acad. Sci. U.S.A.* **1999**, *96*, 361. (b) Kröger, N.; Lorenz, S.; Brunner, E.; Sumper, M. *Science* **2002**, *298*, 584.
(23) (a) Yamada, K.; Shosenji, H.; Ihara, H. *Chem. Lett.* **1979**, *8*, 491. (b) Smith, G. D.; Barden, R. E. *Chem. Phys. Lipids* **1975**, *14*, 1.
(24) Kalyanasundaram, K.; Thomas, J. K. *J. Am. Chem. Soc.* **1977**, *99*, 2039.

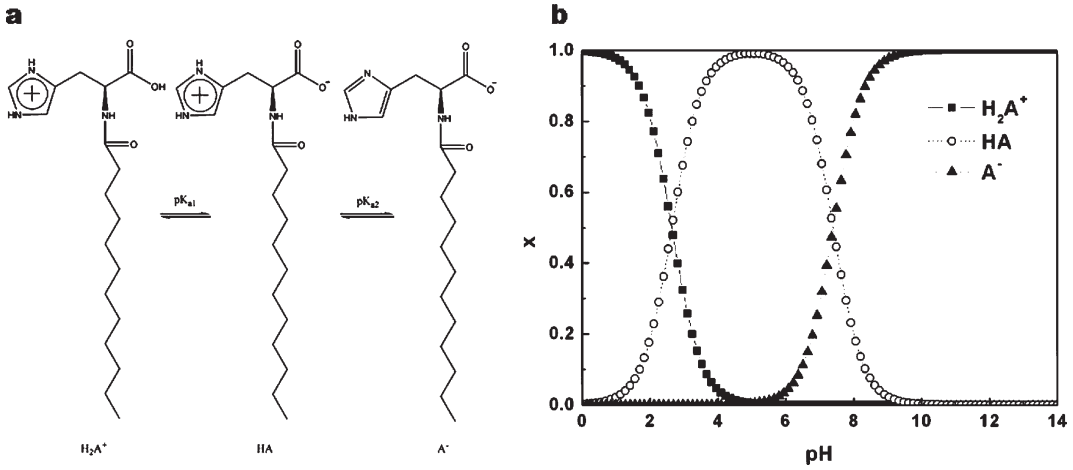

Figure 1. (a) Species transitions during the titration of DHis with HCl. (b) Species distribution of DHis solution within pH range of 0−14 at 30 °C.

foil supported on a copper grid. Nitrogen adsorption and desorption isotherms were measured using a Micromeritics ASAP 2010 system at −196 °C. Samples were degassed at 350 °C overnight under vacuum (10^{-5} Torr). The pore size distribution was calculated from the adsorption branch of the isotherm by the Barrett−Joyner−Halenda (BJH) method, and the specific surface area was obtained by the Brunauer−Emmett−Teller (BET) method. Each of the results had been repeated three times to give the average values. The steady-state fluorescence spectrum was measured with a FLS 920 spectrofluorometer of Edinburgh Instruments using a monochromated Xe lamp as an exitation source. Time-resolved fluorescence spectrum measurement was performed with a Lifespec Red spectrofluorometer of Edinburgh Instruments equipped with a Hamamatsu picosecond light pulser C8898 using 393 nm laser with a repetition rate of 1 MHz as light source. For each measurement, at least 3000 photon counts were collected in the peak channel to ensure the decay quality. The goodness of fit of decay curves, χ^2, was no more than 1.3. For the fluorescence measurements of silica nanotubes, a cell made of quartz glass was used as solid sample container.

Results and Discussion

1. Macro- and Microscopic Observations of Aqueous DHis Solution by Ionic Surfactants Solubilization. A histidine derivative surfactant DHis was synthesized, and its basic chemical properties were investigated. As shown in Figure S4 in the Supporting Information, DHis (denoted as HA) was a pH-responsive zwitterionic surfactant with two pK_a values (2.65 and 7.40), which could transform into its cationic (H_2A^+) or anionic form (A^-) in acidic and basic solution (Figure 1a), respectively. By adjusting pH, the components of DHis molecular species in aqueous solution could be tuned, as illustrated in Figure 1b.

The zwitterionic nature of histidine headgroup endowed the three species of DHis molecule with different solubility and aggregation ability. Figure S5 in the Supporting Information showed the variation of pyrene I_1/I_3 with the concentration of DHis at different pH values, which was utilized to estimate the cac value of each system. It was clearly seen from the results listed in Table 1 that the solubility and aggregation ability of species H_2A^+ and A^- were better than the neutral form HA. In fact, at 30 °C, HA was insoluble in water at pH 5.02, which was its isoelectric point (pI). Thus, addition of another ionic surfactant, which could play similar role of species H_2A^+ and A^-, was expected to improve HA solubility at pI by surfactant solubilization.

However, when mixing DHis with conventional cationic surfactant DTEAB at 30 °C (the pH for the mixed surfactants was

Table 1. Critical Aggregation Concentration (cac) in Acidic and Basic DHis Solution Determined by Steady-State Fluorescence Measurement

	molar ratio of species (%)					
system	H_2A^+	HA	A^-	exptl temp (°C)	cac (mmol/L)	precipitation concn at 30 °C (mmol/L)
pH = 1.85	86	14	0	45	4.2	2.0
pH = 2.65	50	50	0	45	1.6	0.4
pH = 7.40	0	50	50	45	2.0	0.6
pH = 12.0	0	0	100	45	13	no precipitates

at the range of 4.9−5.2), an interesting dynamic phase behavior transition over time (Figure 2a) could be observed. The appearance of the mixed system transformed from transparent solution to opalescent gel and finally into flocculent precipitate. By varying the mixing ratio of DHis to DTEAB, the final appearance of the system after aging (Figure 2b) evolved from precipitate to flocculent precipitate (with DHis/DTEAB equaling to 9/1, 8/2, 7/3, 6/4, 4/6, and 2/8) and finally to clear homogeneous solution (with DHis/DTEAB of 1/9). The amount of floccules which was apparently visualized as bundles of centimeter-long white fibers decreased with increasing DTEAB amount (Figure 2b). It needs to be mentioned that the dynamically growing fiber systems appeared to be metastable: the gel state during phase transition process depended on the midway process such as cooling rate. For example, the freshly prepared solution was homogeneous when heated to 80 °C. In the first cooling cycle it became jellylike and finally shrank and precipitated from the solution. When the solution was heated to 80 °C again and cooled in the second cycle, it immediately precipitated to be floccules, without a gel state in the midway. So the sol−gel transition temperature (around 50 °C) could not be reproduced for the same sample in repeating cycles as shown in Figure S6 in the Supporting Information. In other compositions such as DHis/DTEAB = 2/8 and 1/9, there was not gel state in the midway, and the sol−gel transition could not be observed.

Characterization of SEM, TEM, and HRTEM (Figure 2c−e) revealed that in the DHis/DTEAB = 8/2, C_t = 10 mM system, the opalescent gel formed in freshly prepared solution was made up of fibers with an exterior diameter in the range of 30−50 nm. And the floccules, which were shrinked out from the aged stock solution, consisted of intertwisted fibers with diameter of hundreds of nanometers. While the aggregates in the clear homogeneous

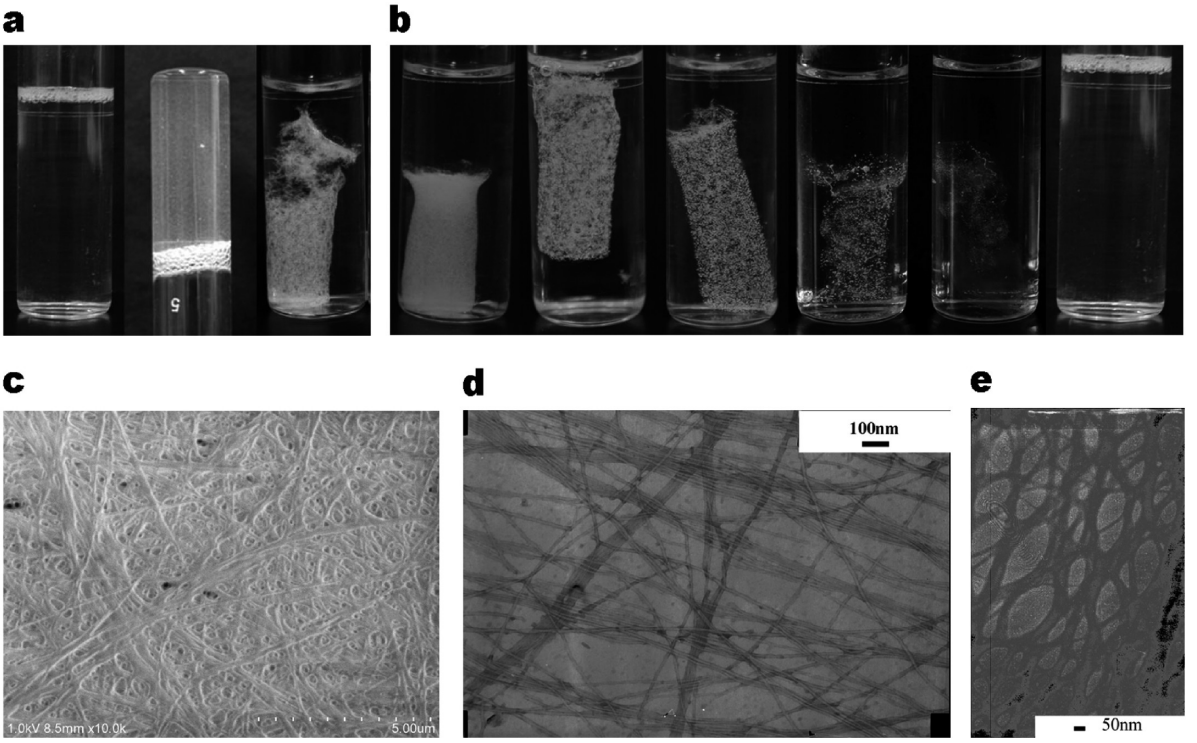

Figure 2. (a) Phase behavior transition of DHis/DTEAB = 8/2, C_t = 10 mM solution over time when freshly prepared, after 2 h and after 1 day, respectively, incubated at 30 °C. (b) Appearance of DHis/DTEAB = 9/1, 8/2, 7/3, 6/4, 4/6, 2/8, and 1/9, respectively, C_t = 10 mM, incubated at 30 °C after 1 day. (c) SEM image of bluish precipitates from DHis/DTEAB = 8/2, C_t = 10 mM solution incubated at 30 °C after 1 day. (d) TEM and (e) HRTEM images of opalescent gel formed in freshly prepared DHis/DTEAB = 8/2, C_t = 10 mM solution.

solution in the DHis/DTEAB = 1/9, C_t = 10 mM system were primarily vesicles with diameters of hundreds of nanometers (Figure S7 in the Supporting Information). The dynamically evolutionary process indicated that the fibrous aggregates in the system were in a metastable state which could undergo an intertwisted growing dynamics during the aging period. This phenomenon seems to be a common feature of aromatic amino acid surfactants[25] which may origin from the controlled recrystallization process of the surfactant in hydrophilic and hydrophobic metastable balance.

Furthermore, similar dynamic phase behavior could be found in the SDS and DHis mixed system, and the microscopic structures were almost the same as the DHis/DTEAB system. It should be noted that in the DHis/SDS system the fibrous aggregates were negative charged, whereas in the DHis/DTEAB system they were positive charged.

Thus, we have obtained dynamic growing and surface charge tunable fibrous aggregates in a simple manner. By virtue of acid and alkali free strategy, the catalytic activity of exposed protonable imidazole groups to the hydrolysis and condensation of silica precusors would ensure the system a promising template for silica growth in a self-catalytic manner.[26] So the refined system was adapt to be utilized as dynamic template in the sol−gel fabrication of silica nanostructures. In fact, similar phase behavior and dynamic growing fibrous aggregates could also be acquired merely by pH regulation instead of ionic surfactants solubilization. But in this way the system would be affected by carbon dioxide in air which may cause the template collapsed during incubation. Therefore, we introduced the ionic surfactants solubilization system as template in the sol−gel process to produce silica nanomaterials, which may have advantages in both simplifying the synthetic procedure and ensuring high yield synthesis.

2. Fabrication of Size-Tunable Silica Nanotubes by Synergetic Growth of Both Template Fibers and Silica Precursors. Applying the fibrous molecular assemblies of the DHis/DTEAB system as templates, we utilized the sol−gel strategy to obtain well-defined silica nanotubes with controlled size, in a simple manner without additional acidic or basic catalyst. In order to investigate the interactions of silica precursors with template fibers, TEOS was added into freshly prepared DHis/DTEAB solution, i.e., at the early stage of the fibrous precipitates growing process. Thus, the hydrolysis and condensation of silica precursors were synergistically underwent at the same time when the fibrous aggregates were growing thicker and more intertwisted. We have tried the composition DHis/DTEAB of 8/2, 6/4, 4/6, and 1/9 as templates for the synthesis of silica nanostructures. From the images in Figure S8 in the Supporting Information, we can conclude that silica nanotubes could be acquired by using DHis/DTEAB of 8/2, 6/4, and 4/6, among which the template of DHis/DTEAB = 8/2 could provide the most favorable (uniform in diameter) nanotubes. So the composition DHis/DTEAB = 8/2 is employed as the template for the synthesis of silica nanotubes. It is to be emphasized that the morphology of the silica gel prepared templating DHis/DTEAB = 1/9 was dramatically changed to be hollow sphere with diameter of several micrometers (Figure S8d in the Supporting Information).

The synthetic silica nanotubes are of high yield (most of the synthesized materials were in the shape of nanotube; see Figure S9 in Supporting Information) and well-defined with homogeneous inner and outer average diameters of 10 ± 2 and 30 ± 5 nm, respectively (Figure 3a,d). SEM and HRTEM images (shown in Figure 3) revealed that by simply varying incubation temperature, the as-synthesized silica nanotubes resulted in different pore size

(25) Ohta, A.; Danev, R.; Nagayama, K.; Mita, T.; Asakawa, T.; Miyagishi, S. *Langmuir* **2006**, *22*, 8472.
(26) Yuwono, V. M.; Hartgerink, J. D. *Langmuir* **2007**, *23*, 5033.

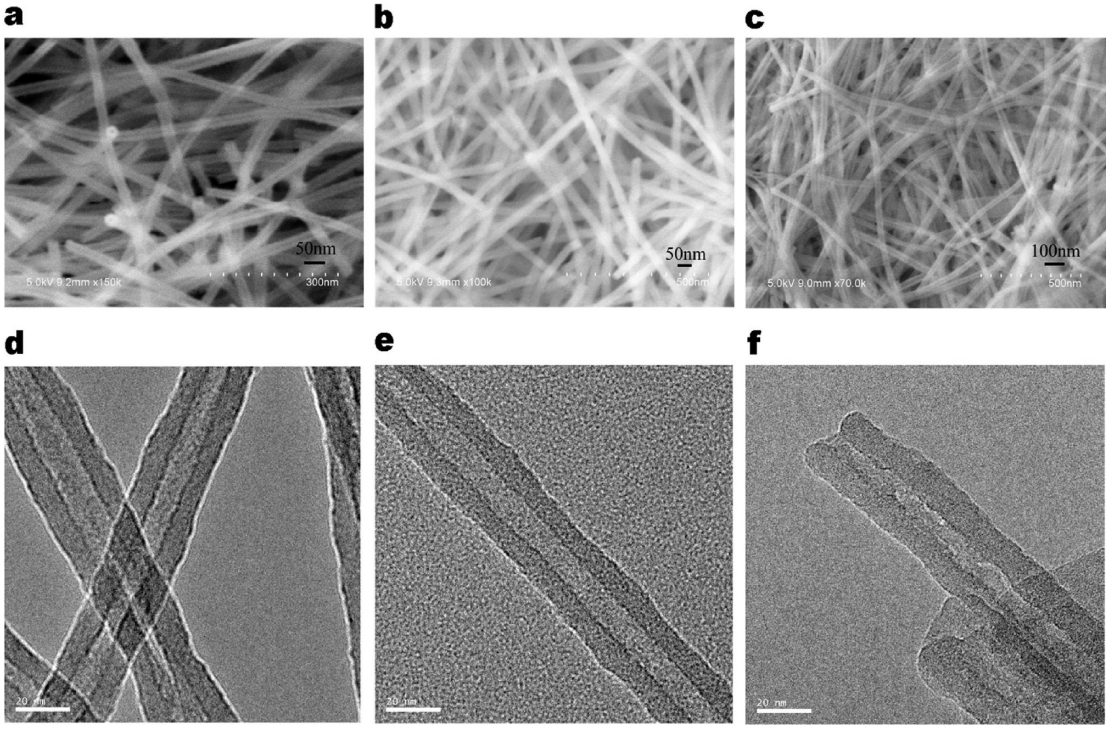

Figure 3. SEM photographs of silica nanotubes after calcination synthesized in DHis/DTEAB = 8/2, C_t = 10 mM system, incubated at (a) 20, (b) 25, and (c) 30 °C. HRTEM photographs of silica nanotubes after calcination synthesized in the DHis/DTEAB = 8/2, C_t = 10 mM system, incubated at (d) 20, (e) 25, and (f) 30 °C.

and uniform wall thickness. Low-temperature (20 °C) synthesis is prone to get thinner (outer diameter ~26 nm, inner diameter ~8 nm) and much uniform nanotubes (wall thickness ~10 nm). It is worth noting that the wall thickness seems to keep constant (ca. 10 nm) at variable temperature, showing the self-catalysis nature of the fiber surface in the process of silica coating and deposits. However, in order to get favorable nanotubes, the synthesis process in the Experimental Section has to be carefully optimized. For instance, the initial concentration of TEOS affects the quality of synthetic nanotubes, as shown in Figure S10 in the Supporting Information. The synthesis is preferred to be conducted at a TEOS concentration less than 5%. Similarly, we have performed the synthesis for different incubation time, such as 6 h, 18 h, 24 h, and 3 days (data not shown), and found that 1 day incubation could provide the preferred nanotubes. Actually, silica nanotubes can only be obtained below 40 °C; high-temperature (50 °C) synthesis is prone to get silica hollow spherical nanostructures with diameter of several micrometers (Figure S11 in the Supporting Information). This result indicates that under this circumstance the morphology of the template was not one-dimensional fibers anymore, which could not induce the growing of the silica precursors to be confined to one dimension.

3. Characterization of the Properties of Synthetic Silica Nanotubes. The amorphous nature of the silica nanotubes was proved by SAED and its component was confirmed by EDX spectrum. As shown in Figure 4a,b, the ED pattern displaying a diffusive ring reveals that the tubes are amorphous, and the two distinct peaks of silicon and oxygen were observed, indicating the tubes are composed of silica without impurity.

The surface areas and pore size distributions of synthetic silica nanotubes were characterized by nitrogen adsorption and desorption measurements. From Figure 5a, the BET adsorption−desorption isotherms of the three silica samples can be ascribed to type IV hysteresis loop, indicating the presence of mesopores on the walls of silica nanotubes. The BET specific

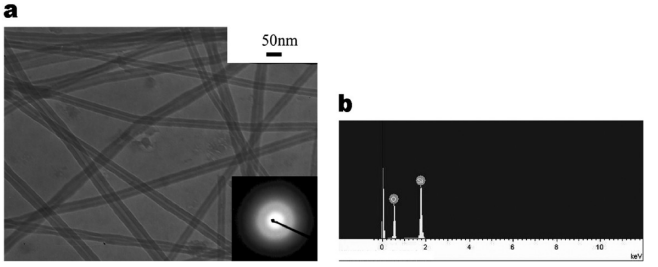

Figure 4. (a) TEM image (inset: ED pattern) and (b) EDX spectrum of silica nanotubes after calcination templating DHis/DTEAB = 8/2, C_t = 10 mM incubated at 25 °C.

surface areas of the mesoporous silica nanotubes were averaged 332, 404, and 341 m^2/g for synthetic temperature of 20, 25, and 30 °C, respectively, which are at a good level for silica nanostructures in the literature.[27] Furthermore, deduced from the isotherms, the BJH pore volume and the average pore size of the three samples were increased with increasing incubation temperature, as shown in Figure 5b and Table 2. Thus, the results derived from the nitrogen adsorption−desorption data are consistent with the microstructure revealed by SEM and HRTEM images.

Interestingly, the photoluminescence (PL) properties of the as-calcined silica nanotubes was also investigated and interpreted herein. Figure 6 shows photographs of the synthetic silica nanotubes owning optical properties. We can see that under irradiation of 365 nm ultraviolet light the nanotubes could emit strong visible light in dark, among which the 25 °C sample showed the strongest luminescent property. After removal of UV light, a residual blue light was luminized from the silica materials decaying for seconds. Taking the 25 °C sample for example, from the solid powder PL spectrum (Figure 7a), we can see that with a

(27) Che, S.; Liu, Z.; Ohsuna, T.; Sakamoto, K.; Terasaki, O.; Tatsumi, T. *Nature* **2004**, *429*, 281.

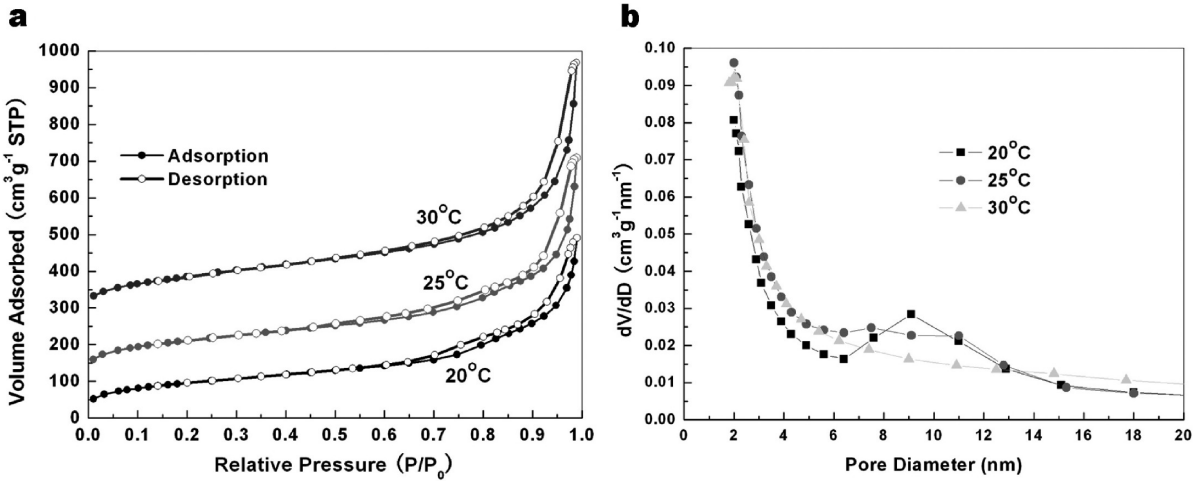

Figure 5. (a) Nitrogen adsorption−desorption isotherms of as-prepared silica nanotubes at different incubation temperature (Isotherms of 25 and 30 °C have been offset by 100 and 300 cm^3/g, respectively, along the vertical axis for clarity; STP: standard temperature and pressure). (b) BJH adsorption pore volume distribution curves of as-prepared silica nanotubes at different incubation temperatures.

Table 2. Diagram for the Surface Properties of the Synthetic Silica Nanotubes

incubation temp (°C)	BET surface area (m^2/g)	BJH pore vol (cm^3/g)	av pore diam (nm)
20	332 ± 21	0.74 ± 0.03	8.6 ± 0.1
25	404 ± 12	0.92 ± 0.05	9.6 ± 0.3
30	341 ± 15	1.05 ± 0.04	11.9 ± 0.5

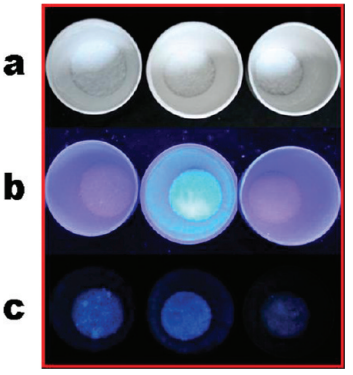

Figure 6. Photograph of the photoluminescent property of the as-prepared silica nanotubes after calcined at 550 °C: (a) under day light, (b) irradiated by 365 nm UV light, and (c) after radiation of UV light and removing light source (incubation temperature from left to right: 20, 25, and 30 °C).

maximum excitation wavelength of 340 nm (3.65 eV) two distinct fluorescence emissions peaks at 400 nm (3.10 eV) and 460 nm (2.70 eV) are generated. The PL property of silica nanostructures is still an open topic that has not reached a current consensus. Commonly, it is believed that the violet light emission at 400 nm is ascribed to some intrinsic diamagnetic defect centers, such as the 2-fold-coordinated silicon lone pair centers (O−Si−O), and the blue light emission at 460 nm is attributed to the neutral oxygen vacancy (≡Si−Si≡).[28] In fact, oxygen vacancies of the silica materials originate during the sample preparation process and give rise to the structural defects, which results in radiative recombination centers for the observed PL bands. It should be addressed here that the PL feature of the synthetic silica nanotubes is very identical, which could be obtained from the entire silica nanotubes.

In addition, we also investigate the PL decay dynamics of the 25 °C sample (Figure 7b). In agreement with previous reports,[29] the PL decay of this sample is not pure exponential, implying a complex relaxation dynamics. In the present case, the transient emission can be well fitted by a double-exponential function:

$$I(t) = A_1 \exp(-t/\tau_1) + A_2 \exp(-t/\tau_2) \quad (1)$$

where τ_1 and τ_2 are the fast- and slow-decay components, respectively, while A_1 and A_2 are the pre-exponential factors. The parameters deduced from the function show a slow-decay time constant of 14.4 ns and a fast-decay time constant of 2.80 ns. Uchino and co-workers[29a] interpreted that the slow-decay component results from trapping and detrapping process associated with certain pore surfaces states, whereas the fast-decay component represents the effective radiative lifetime of the electron−hole recombination process of the germane emission centers possibly in the form of the defect pairs. The PL decay dynamics of our synthetic silica nanotubes can be ascribed similarly to their explanation. We have also examined the PL decay time data including the other two incubation temperature (Figure S12 in the Supporting Information) and found that the curves of 20 and 30 °C were similar in shape and different from that of 25 °C. From Table S1 in the Supporting Information, we can conclude that the fast-decay time constants of the other two temperature were 1 order of magnitude smaller than that of 25 °C. However, whether the decay time constant depends on size and morphology of silica nanotube seems still an open question that needs further examination.

4. Synergetic Growth Mechanism of the Feedback Actions between the Template Growth and Inorganic Deposition Driven by Electrostatic Neutralization. In order to uncover the interaction between silica precursors and template, controlled experiments have been done. When employing the DHis/SDS system instead of the DHis/DTEAB system, negative charged fibers were acquired. In this case, TEOS could not hydrolyze and condense on the surface of fibers completely due

(28) (a) Kohketsu, M.; Awazu, K.; Kawazoe, H.; Yamane, M. *Jpn. J. Appl. Phys.* **1989**, *28*, 615. (b) Tohmon, R.; Ohiki, Y.; Sasagane, K.; Nagasawa, K.; Hama, Y. *Phys. Rev. B* **1989**, *39*, 1337.

(29) (a) Nakazaki, Y.; Fujita, K.; Tanaka, K.; Uchino, T. *J. Phys. Chem. C* **2008**, *112*, 10878. (b) Banerjee, S.; Datta, A. *Langmuir* DOI: 10.1021/la902265e.

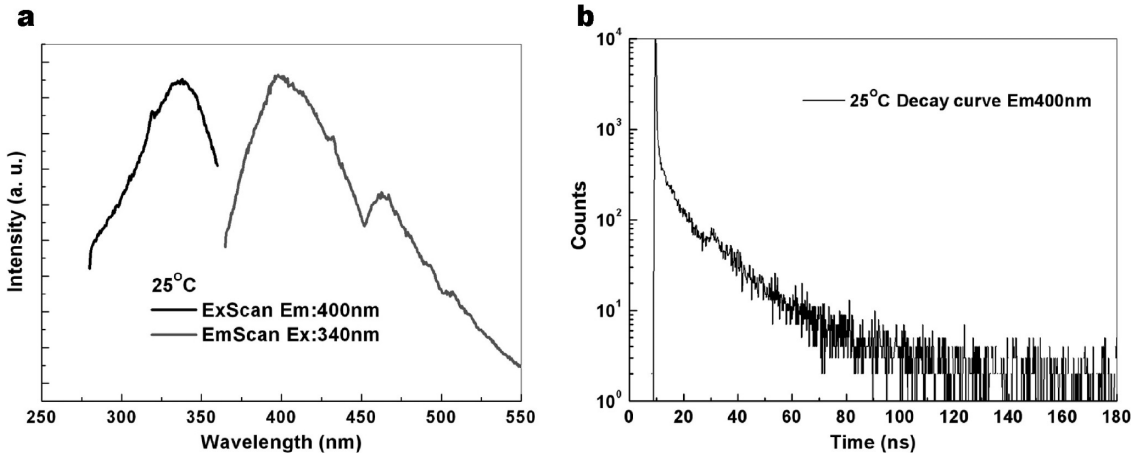

Figure 7. Steady-state photoluminescence (PL) spectra (a) and PL decay curves (b) for the silica nanotubes incubated at 25 °C, after calcination.

Scheme 1. Schematic Representation of Synergetic Growth Mechanism of Silica Nanotubes Fabricated by the Sol−Gel Template Approach

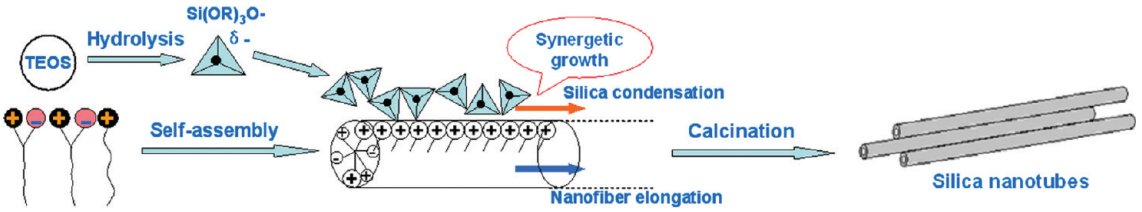

to electrostatic repulsion as the silica precursors are slightly negatively charged in this situation. As expected, only a tiny amount of products were obtained with hollow spherical morphology. A conclusion is easily drawn from the result that opposite charge neutralization is the fundamental requirement for this process.

Another controlled test was operated by addition of TEOS to the DHis/DTEAB system after 1 day's incubation when the visible flocculent precipitate already formed. The resultant silica nanotubes were of low yield and poor quality in uniformity (large quantity of unreacted TEOS oil remained in the upper phase of the stock solution after 2 days). This result suggested the synergetic nature of the process that if the template had been already fully intertwisted, it could not provide enough surface area to control the growth of the silica precursors efficiently.

Thus, we proposed a dynamic template mechanism based on two distinct self-assembly process occurring simultaneously: the nanofiber organic template formation and the surface-confined condensation of silica. On the one hand, the silica polymerization is activated by the enrichment of imidazole headgroup on the surface of the fibers, whereas in the bulk solution the monomer concentration of DHis molecule was at low level (< 1 mmol/L). On the other hand, the assembly/ disassembly equilibrium of fibers is shifted toward the formation of detached long nanofibers by the continuous neutralization of the reformed template. In summary, the local coupling of the self-assembly processes derived from two cross-linked feedback mechanisms at the molecular scale, involving Coulomb interactions between the two oppositely charged building blocks, namely silicates and the surfactant monomers. The synergetic coupling of the two processes requires a mutual feedback, which promotes both nanofiber elongation and silica condensation during the reaction time span (Scheme 1). The regularity of the nanotube wall thickness strongly supports the idea that the two processes are intimately interwoven. The mineralization reaction generally leads to a slightly negatively charged silica deposit due to unreacted silanol groups.[30] Hence, the hybrid nanotubes are obtained with well-defined deposit thickness, preventing further catalysis of the condensation. The neutralization of Coulomb interaction is therefore the underlying principle governing synergistically the surface-confined condensation of silica onto tubes of uniform thickness. Here, the classical static template mechanism has been excluded, whereas the dynamic template offers the unique opportunity to generate architectures far beyond the initial size of the template.

5. Versatility for Construction of Titania Nanotubes Using Negative Charged Self-Assembled Fibers as Template. Enlightened by the intrinsic Coulomb neutralization nature of the strategy, we enlarged the application field of our template by fabrication of functional metal oxide nanotubes such as titania in DHis/SDS negatively charged fibers system. Despite TBOT is not as an idea precursor as TEOS for sol−gel process in aqueous media due to its extremely fast hydrolysis rate, we achieved synthesis of titania nanotubes by conducting the process at low temperature (20 °C) and using TBOT modified with the same molar of ACA as the titanium source. Under these conditions, the hydrolysis and condensation rate of titania precursors could be slowed down matching with the growth of fibers in this system. Only in this case could the partially hydrolyzed, positively charged TBOT precursors be directed into the surface of the negatively charged fibers via electrostatic interactions. SEM and TEM images reveal that the synthetic titania nanotubes are poly dispersive in outer diameter from 30 to 80 nm (Figure 8a,b). SAED and EDX results suggest that the nanotubes are of polycrystalline nature and composed of purely titanium and oxygen with a molar ratio of approximately 1:2 (Figure 8b,c). To the best of our knowledge, there have been few reports about

(30) Brinker, C. J.; Scherer, G. W. *Sol-Gel Science. The Physics and Chemistry of Sol-Gel Processing*; Academic: New York, 1990.

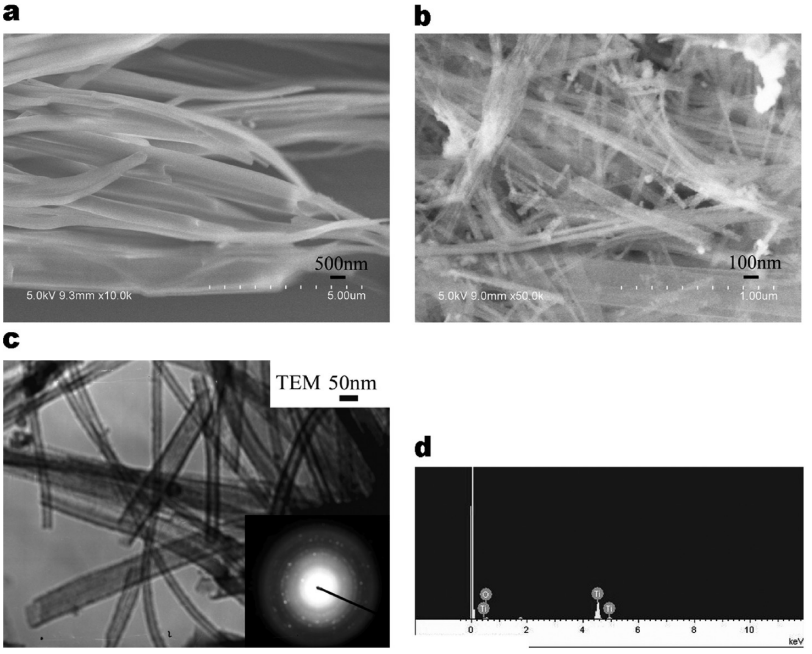

Figure 8. SEM images of synthetic titania nanotubes using DHis/SDS = 8/2, C_t = 10 mM as template and TBOT/ACA = 1/1 as precursor before (a) and after (b) calcination at 500 °C, (c) TEM image (inset: ED pattern), and (d) EDX spectrum of calcined titania nanotubes using DHis/SDS = 8/2, C_t = 10 mM as template and TBOT/ACA = 1/1 as precursor.

titania nanotubes sol−gel synthesis in aqueous media[31] since the hydrolysis and condensation rate of titania precursors are too fast to be controlled. The route herein may enlarge the sol−gel synthetic approach of titania nanotubes under mild conditions, which is anticipated to find applications such as dye-sensitized solar cells.[32]

Conclusion

Formation and growth of fibrous aggregates were studied in an amino acid derivative surfactant DHis system. By ionic surfactants solubilization, surface charge tunable fibrous aggregates could be obtained and then served as versatile template for opposite charged precursors in the preparation of silica and titania nanotubes. The production was in high yield, and the synthetic silica nanotubes were of tunable size and uniform wall thickness, owning good specific surface area and displaying peculiar photoluminescence property. The mechanism underlying the sol−gel replication procedure was put forward as synergistically surface-confined condensation of corresponding precursors on fiber surface driven by Coulomb interactions. Although the complexity of biological systems is not achieved in the reported case, it also provides a further insight into fundamental mechanisms possibly occurring in biological hierarchical architectures. Considering the process occurred in aqueous solution, this methodology is beneficial to application in environmental benign media. We hope that our refined synthetic model system will open possibilities to design and produce other functional materials under mild condition via so-gel procedure for biological and technological applications.

Acknowledgment. This work was supported by National Natural Science Foundation of China (20873001, 20633010, 20976003 and 50821061) and National Basic Research Program of China (Grant 2007CB936201). We thank the Center for Biological Electron Microscopy and the Electron Microscopy Laboratory of the Department of Physics, Peking University, for electron microscopy work.

Supporting Information Available: Details for the synthesis of DHis, ^{1}H NMR, and ESI-MS spectrum of DHis, determination of pK_a of DHis molecule in aqueous solution, determination of cac of DHis by steady-state fluorescence technique, determination of sol−gel transition temperature by DSC, aggregates of DHis/DTEAB = 1/9, C_t = 10 mM system at 30 °C, influence of the template composition to the morphology of silica nanostructures, large-scale SEM images of synthetic silica nanotubes, influence of initial concentration of TEOS on the quality of synthetic nanotubes, SEM images of silica hollow spheres prepared at 50 °C, and PL decay kinetics of synthetic silica nanotubes at different incubation temperature. This material is available free of charge via the Internet at http://pubs.acs.org.

(31) (a) Adachi, M.; Murata, Y.; Harada, T.; Yoshikawa, S. *Chem. Lett*. **2000**, 942. (b) Peng, T.; Hasegawa, A.; Qiu, J.; Hirao, K. *Chem. Mater*. **2003**, *15*, 2011.

(32) Haque, S. A.; Palomares, E.; Cho, B. M.; Green, A. N. M.; Hirata, N.; Klug, D. R.; Durrant, J. R. *J. Am. Chem. Soc*. **2005**, *127*, 3456.